Active Dendrites Reduce Location-Dependent Variability of Synaptic Input Trains

ERIK P. COOK AND DANIEL JOHNSTON
Division of Neuroscience, Baylor College of Medicine, Houston, Texas 77030

Cook, Erik P. and Daniel Johnston. Active dendrites reduce location-dependent variability of synaptic input trains. *J. Neurophysiol.* 78: 2116–2128, 1997. We examined the hypothesis that dendritic voltage-gated channels can reduce the effect synaptic location has on somatic depolarization in response to patterns of short synaptic trains (referred to as *location-dependent variability*). Three computer models of a reconstructed hippocampal CA1 cell, each of increasing realism and complexity, were used. For each model, the goal was to identify the dendritic composition that best reduced the location-dependent variability. The first model was linear and a single parameter, dendritic membrane conductance (G_{D_m}, where $R_m = 1/G_{D_m}$), was varied. Surprisingly, a negative G_{D_m} minimized the location-dependent variability. Superposition of the synaptic inputs showed that, compared with passive dendrites, active dendrites increase the mean of the individual responses while decreasing the variance between synapses at different locations. Active dendrites compensate the three components of passive cable signal interference that increase with distance from the soma: the accumulation of charge on dendritic membrane capacitance, the escape of charge across synaptic and nonsynaptic dendritic membrane conductances, and the reduction in synaptic charge entry due to increased depolarization of dendrites located farther from the soma. We also found that the entire active dendritic tree contributes charge to any one active synapse. The second model contained an artificial voltage-dependent current (I_{boost}) added to passive apical dendrites. The optimal amount of I_{boost} that minimized location-dependent variability was found to be independent of the strength of individual synaptic inputs but inversely related to the synaptic duration. In the third model, realistic T-type Ca^{2+} and persistent Na^+ channel models were added to passive dendrites and numerically fit to reproduce the effects of I_{boost}. Both realistic currents minimized synaptic variability. The densities for the realistic dendritic currents were not uniform but showed subtle variations and a slight reduction with distance from the soma. A heteroassociative memory network also was modeled to demonstrate the important relationship between location-dependent variability and memory recall performance. Compared with passive dendrites, active dendrites increased memory storage by reducing recall errors. These simulations demonstrate that active dendrites can minimize the cable properties of passive dendrites and enhance the soma's ability to determine the strength of the synaptic input. These models predict dendrites that minimize location-dependent variability will have an overall negative slope conductance *I-V* relationship that is tuned precisely.

INTRODUCTION

Wilfrid Rall's (1959) passive theory of dendrites predicts that a synapse's effectiveness at the soma is dependent on its location (referred to as location-dependent variability). It, however, has long been hypothesized that dendritic voltage-gated channels may counteract this property and make all synapses electrotonically equidistant from the soma (Andersen et al. 1980; Jack et al. 1975; Johnston et al. 1996; Shepherd et al. 1985). This is known as the ''boosting hypothesis'' of active dendrites because it implies distal inputs are amplified selectively (Crill 1996; Lorente de Nó and Condouris 1959; Rall 1970; Schwindt and Crill 1995). If we assume that the boosting hypothesis is correct, then what predictions can be made regarding the properties of dendrites that would eliminate the effects of synaptic location on somatic response? What would the dendritic *I-V* relationship be? And how might dendritic voltage-gated channels produce this effect?

The role of dendrites in synaptic integration is a topic of much debate and intensive experimental and theoretical studies. With recent experimental evidence indicating that dendrites contain a full complement of voltage-gated channels (Hoffman et al. 1997; Magee and Johnston 1995), dendritic function has become the focus of neuronal modeling with many proposing elaborate dendritic computations (Koch et al. 1983; Mel 1993; Segev 1992; Shepherd and Brayton 1987; Woolf et al. 1991). This study departs from these models by assuming that dendrites function as high-fidelity transducers of synaptic input that accurately convert synaptic conductance into somatic depolarization independent of synaptic location. The importance of accurately transferring synaptic input to the soma becomes evident when one considers that most theories of learning and memory place the site of information storage at the synapse.

The passive model of dendrites, however, argues against all synapses being electrically equidistant from the soma (Spruston et al. 1994). Location-dependent variability, resulting from dendritic cable properties, reduces the amount of synaptic charge reaching the soma. First, the amount of synaptic charge injected into the dendrites decreases with distance from the soma. Next, synaptic charge traveling to the soma is reduced as charge escapes across dendritic membrane conductances and accumulates on the dendritic capacitance. The amount of location-dependent variability is confounded further by the synaptic input itself, which can alter drastically the membrane conductance of the dendritic tree (Bernander et al. 1991).

Using computer simulations of a reconstructed CA1 pyramidal cell, the hypothesis that dendritic voltage-gated channels can reduce the effect synaptic location has on the firing response was tested. The goal was to develop a theoretical foundation with simplified models and membrane currents on which realistic channel models could be applied. Three different models, ranging from simple to complex, were used: *model 1*, linear; *model 2*, spiking soma with an artifi-

cial voltage-dependent dendritic current (I_{boost}); and *model 3*, spiking soma with realistic dendritic voltage-gated channels. De Schutter and Bower (1994) have demonstrated that active dendrites in a purkinje cell model can reduce the variability of single excitatory postsynaptic potentials (EPSPs). In this paper, the inputs to our models are short trains of synaptic input, and rather than analyzing a previously designed model, we attempt to find the optimal dendritic configuration that minimizes location-dependent variability.

With all three models, we found that active dendrites reduce the location-dependent variability of synaptic input to the soma. The amount of dendritic excitability necessary to minimize this variability, however, required precise regulation. The importance of accurately transmitting synaptic strength to the soma was demonstrated using a simple heteroassociative memory network (Palm 1980). Active dendrites that reduce the effect of location on synaptic input increased memory recall performance of the network.

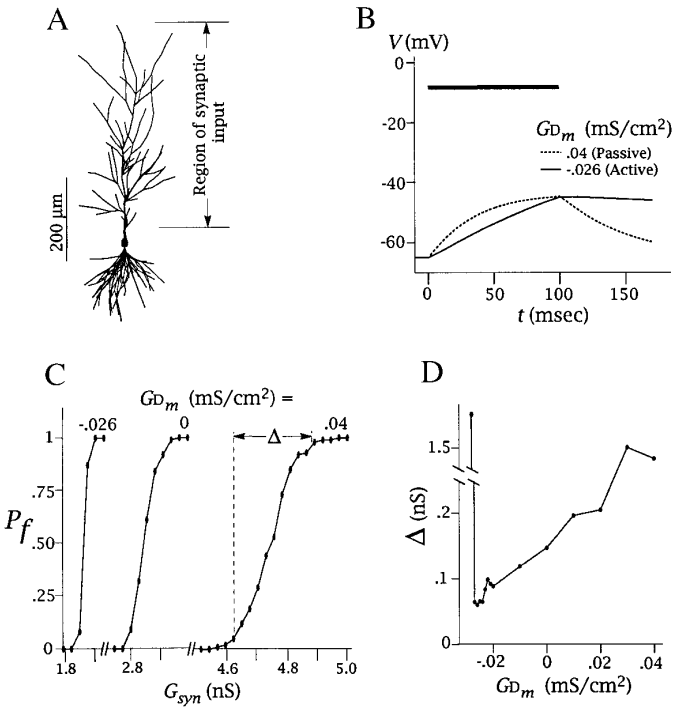

FIG. 1. Minimizing location-dependent variability in a nonfiring CA1 pyramidal model. *A*: compartmentalized version of the CA1 neuron used in the simulations and the region of synaptic input. *B*: an example of the somatic depolarization to a 100-ms synaptic input (heavy bar) for $G_{D_m} = 0.04$ and -0.026 mS/cm^2. Because the soma was passive, an artificial threshold (V_{th}) was arbitrarily defined as -45 mV. If somatic potential reached V_{th}, the model was said to have fired an action potential. Number of active synapses was adjusted in each case to produce the same amount of somatic depolarization for each model. *C*: examples of 3 P_f curves for $G_{D_m} = 0.04$, 0, and -0.026 mS/cm^2 (which corresponds to dendritic R_m of 25, 1, and -38.5 kΩcm^2, respectively). Each curve represents the probability (P_f) that the model reaches V_{th} vs. the total synaptic strength (G_{syn}) in response to a random synaptic input pattern. One hundred different input patterns were used to generate each curve. Negative values of G_{D_m} increase the model's excitability thereby requiring a smaller G_{syn} to reach V_{th}. Δ is the range of G_{syn} over which P_f increases from 5 to 95%. This is a measure of location-dependent variability. *D*: Δ vs. G_{D_m}. Notice that the P_f curve corresponding to a G_{D_m} of -0.026 mS/cm^2 has the smallest Δ.

TABLE 1. *General model parameters*

	Basal	Soma	Apical
Compartments	175	14	177
Area, μm^2	9,945	1,281	11,176
R_m, Ωcm^2	25,000	50,000	see Table 2
C_m, μF/cm^2	2	1	2
R_i, Ωcm	200	200	200

METHODS

The reconstructed CA1 pyramidal cell used was provided by D. Turner and is shown in compartmentalized form in Fig. 1*A*. The neurophysiological modeling program NEURON was used for all simulations (Hines 1993). Table 1 lists the general parameters of the model. Unless otherwise indicated, these parameters were used in all simulations. The passive parameters were chosen to provide a membrane time constant (τ_m) of 50 ms. To account for the lack of explicitly modeled spines in the dendrites, R_m was halved and C_m doubled in the apical and basal dendrites (Spruston et al. 1993). The basal dendrites were always passive, whereas the properties of the apical dendrites varied between models.

Differences between the three models are summarized in Table 2. For *models 2* and *3*, a fixed density of fast Na^+ ($\bar{g}_{Na} = 0.05$ S/cm^2) and delayed-rectifier K^+ ($\bar{g}_{KDR} = 0.012$ S/cm^2) conductances were assigned to the soma compartments to always ensure an action potential for the different dendritic conditions. The apical dendrites of *model 2* contained the artificial voltage-dependent current, I_{boost}, which is illustrated in the *inset* of Fig. 5*A*. *Model 3* had either T-type Ca^{2+} (I_{CaT}), persistent Na^+ (I_{NaP}), or both currents in its apical dendrites. The channel densities for the apical dendrites were the parameters of interest and were varied in this study. Channel descriptions are reported in the APPENDIX except for the T-type Ca^{2+} channel, which was previously described in Jaffe et al. (1994).

One thousand synapses were placed uniformly with respect to surface area in the apical dendrites (Fig. 1*A*). Synapses were modeled as either steady-state conductances or α functions with a time to peak of 2 ms and a peak conductance of 100 pS (see Table 2). The synaptic reversal potential was 65 mV above rest. All synaptic input was assumed to be α-amino-3-hydroxy-5-methyl-4-isoxazolepropionic acid (AMPA)-like. Patterns of synaptic input were produced by randomly selecting synapses to be activated. Spines were not included in the model because preliminary simulations suggested they had little effect on the electrical properties of the model.

Details of the numerical fitting of realistic channels to I_{boost} is described in the APPENDIX.

RESULTS

Dendritic fidelity in the linear model (model 1)

In the first model, the dendritic R_m was allowed to assume negative values. We therefore decided to call this the *linear*

TABLE 2. *Model specific parameters*

	Model 1	Model 2	Model 3
Title	Linear	Boosting	Realistic
Apical R_m, Ωcm^2	Varied	25,000	25,000
Composition of soma	Passive	I_{Na} and I_{KDR}	I_{Na} and I_{KDR}
Composition of apical	Passive	I_{boost}	I_{CaT}, I_{NaP}, or both
Synaptic input	Steady state	Train of α functions	Train of α functions

model. This allows a distinction between a positive dendritic R_m that leaks current and is passive and a negative R_m that injects current and is active. The goal was to determine if active dendrites produced by making R_m negative could more accurately transmit the strength of the synaptic input to the soma. Each individual synaptic input (g_s) was modeled as a constant conductance of 27.2 pS,[1] which was chosen to keep all simulations consistent.

Figure 1*B* illustrates the somatic voltage response to the synaptic input for passive and active dendrites. G_{D_m}, the dendritic membrane conductance (where dendritic $R_m = 1/G_{D_m}$), was set to 0.04 mS/cm^2 for the passive dendrites and -0.026 mS/cm^2 for the active dendrites. Notice that $G_{D_m} = -0.026$ produces a slow response because the dendritic membrane time constant is very large. The number of active synapses was adjusted for each value of G_{D_m} to produce 20 mV of somatic depolarization at the end of the synaptic input (100 ms). Because the linear model did not produce spikes, an artificial threshold (V_{th}) was assumed to be 20 mV above rest. If the somatic membrane potential reached V_{th}, the model was said to have fired. Whether or not a model fires an action potential in response to synaptic input was the criterion used to evaluate the location-dependent variability.

The first objective was to devise a measurement of location-dependent variability that could be used in all three models. The probability (P_f) of the model reaching V_{th} was computed as a function of the total synaptic input strength (G_{syn}), which was varied by increasing or decreasing the number of active synapses per pattern ($G_{syn} = n \times g_s$, where n = the number of active synapses). The synapses added or deleted were randomly chosen. For a given value of G_{D_m}, a P_f versus G_{syn} curve was generated by adjusting G_{syn} of each randomly selected synaptic input pattern until the threshold of the model was determined. This procedure was repeated 100 times, with all patterns generated randomly. The proportion of patterns (P_f) of strength G_{syn} that produced a somatic depolarization of V_{th} or greater was plotted.

Figure 1*C* illustrates P_f curves for three values of G_{D_m}. The right most curve is for passive dendrites ($G_{D_m} = 0.04$ mS/cm^2). As G_{D_m} was decreased, the curves shifted to the left due to increased excitability of the model. The slopes of the curves also change as G_{D_m} was varied. A $P_f = 1$ corresponds to the soma reaching V_{th} for all patterns. Likewise, for a $P_f = 0$, no patterns of synaptic stimulation caused the soma to reach V_{th}. The interesting region of these curves comes from values of G_{syn} that produced a P_f between 0 and 1, indicating that only a fraction of input patterns caused the soma to reach V_{th}. Failure of some patterns to produce somatic depolarizations of V_{th} must have been due to the location of the activated synapses because at each point, all patterns had the same strength of G_{syn}. A dendrite that completely eliminated the effect of synaptic location would have a P_f curve in the shape of a step function and would be a perfect threshold detector. Such a model would eliminate location-dependent variability and each synapse would be electrically equidistant from the soma. A dendrite that introduced a substantial locational component on the synaptic input would have a P_f curve that slowly rose from 0 to 1 over a large range of G_{syn}. Our measure of location-dependent variability is defined as Δ, which corresponds to the range of G_{syn} that causes P_f to go from 0.05 to 0.95 (Fig. 1*C*). Active dendrites with a G_{D_m} of -0.026 mS/cm^2 produce a P_f curve with a small Δ compared with the model whose dendrites were passive.

For a range of G_{D_m} values, Δ is plotted in Fig. 1*D*. As G_{D_m} is increased in the negative direction, the dendrites become better tuned in their ability to faithfully transmit synaptic input to the soma. The highest fidelity dendrite corresponds to the minimum Δ at $G_{D_m} = -0.026$. Notice that just eliminating the leak conductance alone (by setting $G_{D_m} = 0$) did not minimize Δ. When G_{D_m} assumed a value more negative than -0.027, the dendrites became unstable, resulting in regenerative dendritic depolarization and a total loss of dendritic fidelity.

Contribution of individual synapses to somatic depolarization

Our first model was linear because it contained no voltage-dependent channels and the synapses were modeled using fixed value conductances. This allowed us to use superposition to assess directly the effect a negative G_{D_m} has on individual synaptic contributions to somatic depolarization. We predicted that a model that minimized Δ also would minimize the variance between individual synaptic responses, regardless of dendritic location.

Superposition states that the voltage at any node in a linear network is equal to the sum of the contribution of the individual voltage sources (Director 1975). Therefore, to see the effect of a single synapse, the reversal potential for all other synapses was set to the resting membrane potential. This procedure is not, however, equivalent to applying a single synapse to the dendrites. It is important to emphasize that all synaptic conductances of a particular input pattern remained in the dendrites, but only one had a reversal potential of 0 mV.

For the passive ($G_{D_m} = 0.04$) and optimal active ($G_{D_m} = -0.026$) dendrites, Fig. 2*A* shows the peak somatic response of 1,000 individual synapses as a function of anatomic distance from the soma. The points in Fig. 2*A* were generated by applying random patterns of synaptic input and computing the individual contribution of each synapse to the soma using superposition. Each input pattern used was strong enough to cause the soma to reach V_{th} at the end of the 100-ms synaptic duration (as in Fig. 1*B*). In the passive dendrite model, the influence on the soma from synapses farther away diminished steadily. In the active dendrite model, the decrement was less. Figure 2*B* accentuates the differences between the two models in a histogram of the voltage responses in Fig. 2*A*. Compared with the passive model, the active dendrites clearly produced a narrower distribution of somatic responses. For the active dendrites, the mean response was increased whereas the variance decreased. The coefficient of variation (CV) of individual synaptic responses was computed as a function of G_{D_m} (Fig. 2*C*).[2] Optimal active den-

[1] This value is equivalent to a time-averaged conductance of a synapse modeled with a 2-ms alpha function with a 100 pS peak activated at 50 Hz (Bernander et al. 1991).

[2] Because of dendritic instability, CV was not computed for $G_{D_m} < -0.027$.

drites ($G_{D_m} = -0.026$) produced a greater than fivefold reduction in CV when compared with passive dendrites ($G_{D_m} = 0.04$). This result verifies that the dendritic composition that minimized Δ also minimized the location-dependent variability of individual synapses.

Active dendrites have increased voltage attenuation

Figure 3 shows the peak dendritic membrane potential for each apical compartment in response to the same input pattern used in Fig. 1*B*. The active dendrites ($G_{D_m} = -0.026$) depolarized more than the passive dendrites ($G_{D_m} = 0.04$). Notice that the potential was the same at the soma for both models. The increased depolarization of the active dendrites resulted from additional inward current entering the distal dendrites. From Ohm's Law, this increased current flowing toward the soma causes an increased voltage drop across R_i of the distal dendrites. A negative G_{D_m}, therefore, boosts the dendritic potential and thus increases the amount of voltage attenuation that occurs from the dendrites to the soma.

Active dendrites compensate for synaptic charge loss and accumulation

How does a negative dendritic membrane conductance minimize the effect synaptic location has on somatic response? This question is answered best by examining how

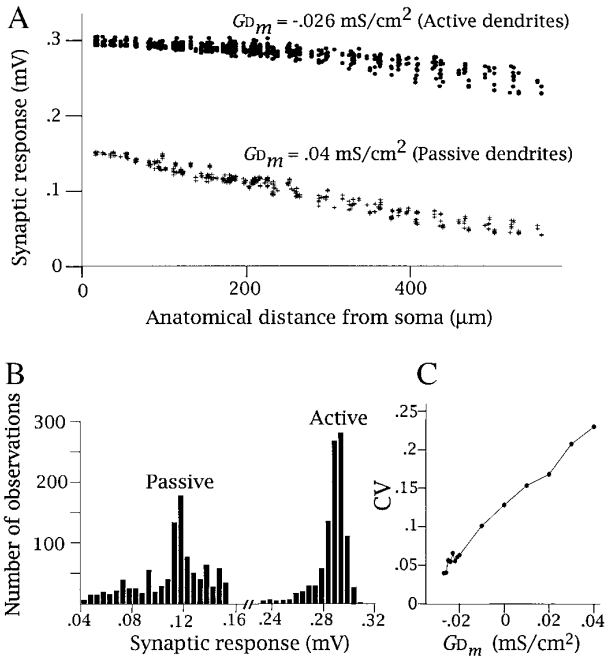

FIG. 2. Effect of active dendrites on individual synapses. *A*: superposition was used to compute the peak somatic response from 1,000 individual synapses. Peak somatic potential is plotted as a function of synaptic distance from the soma. Two models used were a passive model (+) with $G_{D_m} = 0.04$ and the optimal active model (●) with $G_{D_m} = -0.026$. Each data point corresponds to a single synapse, but as there were 1,000 possible synaptic locations in the dendrites, some points may overlap. *B*: histograms of the responses in *A* (binwidth = 0.005 mV). Mean response was 0.11 ± 0.026 (SD) mV for the passive dendrites and 0.29 ± 0. 012 mV for the active dendrites. *C*: coefficient of variation (CV) for the synaptic responses as a function of G_{D_m}. CV of the passive dendrites is >5 times higher than for the optimal active. At values of $G_{D_m} < -0.027$, the dendrites produced regenerative depolarizations, and thus CV was not computed.

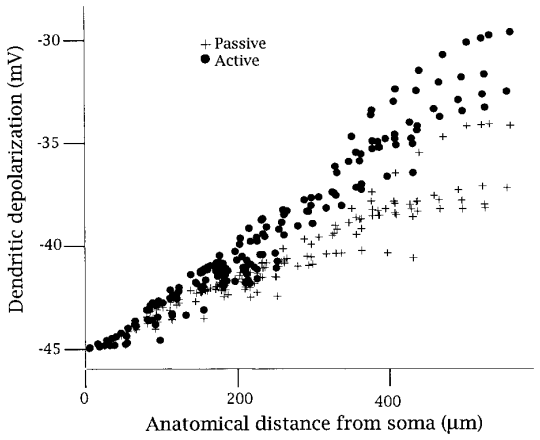

FIG. 3. Synaptic input depolarizes the active dendrite more than the passive. Peak dendritic depolarization is shown in response to a 100-ms synaptic input for the passive ($G_{D_m} = 0.04$) and active ($G_{D_m} = -0.026$) dendrites. Dendritic potential is illustrated as a function of distance from the soma for the passive (+) and active (●) models. Time at which the peak depolarization occurred was slightly different for all dendritic compartments and usually occurred within 1 ms after the synaptic input. Number of active synapses per pattern was adjusted so that the somatic potential in each model reached V_{th} (see Fig. 1*B*).

charge is transferred from the synapses to the soma. Charge transfer has been recognized as an important measure of synaptic strength (Jack et al. 1975; Redman 1976). Examining charge movement provides a clearer picture of the dendrite's effect on the synaptic input than looking at either current or voltage.

In each dendritic compartment of the linear model, current has three *trans*-membrane paths to flow across: membrane conductance, I_g; membrane capacitance, I_c; and synaptic conductances, I_s. If each current is integrated during the 100-ms synaptic input, the net charge transferred across each path can be computed where $Q_g = \int I_g$, $Q_c = \int I_c$, and $Q_s = \int I_s$. This principle is illustrated for a simple three-compartment dendrite in Fig. 4*A*. Conservation of charge requires that the net charge transferred to the soma (Q_{soma}) from the apical dendrites is

$$Q_{soma} = \sum_{i=1}^{n} (Q_{g_i} + Q_{c_i} + Q_{s_i}) \quad (1)$$

where n is the number of dendritic compartments. *Equation 1* can be expressed as the sum of each component of charge transfer or

$$Q_{soma} = \sum_{i=1}^{n} Q_{g_i} + \sum_{i=1}^{n} Q_{c_i} + \sum_{i=1}^{n} Q_{s_i} = Q_g^* + Q_c^* + Q_s^* \quad (2)$$

where Q_g^*, Q_c^*, and Q_s^* represent the net charge transferred by the membrane conductance, capacitance, and synaptic conductance, respectively, for the entire dendritic tree.

Superposition again was used to compute the dendritic contribution of charge to the soma for each active synapse in an input pattern. Figure 4*A* illustrates this idea for a three-compartment dendrite. This figure shows the direction of charge movement when superposition is used to examined the response to a single activated synapse on dendritic compartment 1. Q_s on compartment 1 is the only site of inward

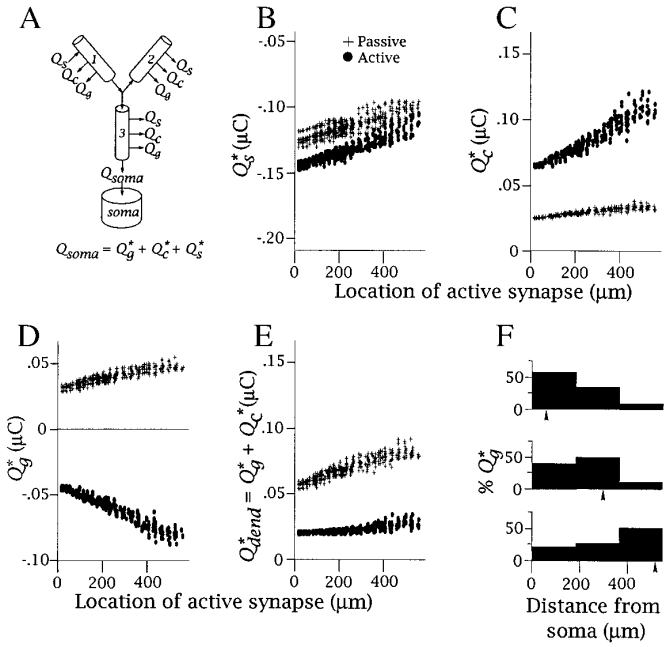

FIG. 4. Active dendrites have uniform charge transfer. Superposition was used to determine the amount of charge movement across the dendritic membrane in response to each individual synapse of an input pattern. Charge escaping across the membrane conductance (Q_g^*), synaptic conductance (Q_s^*), and accumulating on the capacitance (Q_c^*), was computed by integrating the currents associated with each component for the entire dendrite during the 100-ms synaptic input. Net charge transferred to the soma (Q_{soma}^*) is equal to the sum of all charge that passes through ionic conductances less the amount that accumulates on the membrane capacitance. *A*: simple illustration of charge movement when activating a single synapse on compartment 1 in a passive dendrite. Except for the 1 active synapse, the direction of charge movement across the dendritic membrane is outward. *B–E*: charge contribution of the entire dendritic tree vs. the location of each active synapse on passive ($G_{D_m} = 0.04$) and active ($G_{D_m} = -0.026$) dendrites. *B*: total synaptic charge injected into the dendrites decreases as a function of synaptic location. Charge transfer for the passive (+) and active (●) dendrites is shown for the same 1,000 synapses used in Fig. 2. *C*: capacitive charge accumulation increases with synaptic location for both models. Active dendrites have a larger overall accumulation of charge on the membrane capacitance. *D*: passive dendrites have outward charge movement across the membrane conductance, whereas active dendrites inject charge. In both cases, the amount of charge moving across the dendritic conductance increases with the synapses distance from the soma. *E*: dendritic contribution (Q_{dend}^*) is the sum of charge movement and accumulation for the dendritic conductance and capacitance. Active dendrites produce a more uniform charge movement as a function synaptic location. *F*: entire active dendrites contribute to each synapse. For 3 activated synapses (indicated by ↑), the percent charge injected (Q_g) by different regions of the active dendrites is shown. Dendritic regions where the synapses are located contribute only ~50% of the total charge. Regions were determined by dividing dendritic path length from soma into 3 equal sections (proximal, middle, and distal).

charge movement. Note that even though synapses on compartments 2 and 3 have their batteries ''shorted out,'' they still provide a path for charge to escape. For this example, Q_{soma} therefore would be equal to the charge injected on compartment 1 minus the outward movement of charge in the rest of the dendrites. It should be mentioned that although Q_c is illustrated in the same way as other charge movement in Fig. 4*A*, Q_c is in fact not permanently lost. Current in a capacitor is governed by the relationship $I_c = C\,dV/dt$, which provides an inward capacitive current as the dendritic membrane repolarizes back to rest after the synaptic input. The synaptic charge that accumulated on the dendritic capacitance during the 100-ms synaptic input later will be transferred back to the dendrites. However, at the time the model is depolarized enough to fire (at or within a few milliseconds after the synaptic input ends), this charge is unavailable to the soma, and thus we treat it like other charge movement during our finite interval charge calculations in Fig. 4.

Figure 4, *B–D*, illustrates the charge contribution the dendrites make for each individual synapse in the passive ($G_{D_m} = 0.04$) and active ($G_{D_m} = -0.026$) dendrites of the linear model. Superposition was used with the same input patterns and 1,000 synapses as in Fig. 2. In Fig. 4*B*, each point represents the total synaptic charge injected (Q_s^*) as a function of the location of the single activated synapse. (Inward charge, as with inward current, is plotted in the negative direction.) The amount of charge each synapse injected is slightly greater in the active model than in the passive model. With both models, the amount of charge injected decreased for synapses farther from the soma. This was due to the decrease in driving force resulting from increased depolarization of the distal dendrites (as shown in Fig. 3).

The dendritic capacitance accumulated synaptic charge traveling to the soma during the synaptic input (Fig. 4*C*). Each point represents the net charge accumulated on the entire dendritic capacitance (Q_c^*) as a function of an activated synapse's location. Active dendrites had more capacitive charge accumulation than passive dendrites because synapses in the active model produced larger depolarizations (see Fig. 2). Figure 4*D* shows that the greatest difference between the passive and active dendrites is the amount of charge transferred across the membrane conductance (Q_g^*). Passive dendrites lost an increasing amount of charge as synapses were activated farther from the soma. Due to a negative G_{D_m}, active dendrites injected charge during the synaptic input. This charge injection increased with the synapse's distance from the soma.

If $Q_{dend}^* = Q_g^* + Q_c^*$ is defined as the component of the synaptic charge that is either removed or accumulated by the dendritic conductance and capacitance en route to the soma, then Fig. 4*E* illustrates how the negative conductance of the active dendrites increases dendritic fidelity. For passive dendrites, Q_g^* and Q_c^* both increase positively, whereas in the active dendrites, Q_g^* and Q_c^* are related inversely. During the 100-ms interval when synaptic input was present, the passive dendrites subtracted increasing amounts of charge from synapses in a distant dependent fashion. In contrast, the active dendrites subtracted a relatively constant amount of charge, regardless of location.

The net charge transferred to the soma from the apical dendrites (Q_{soma}) is reflected in the peak somatic voltage responses shown in Fig. 2, *A* and *B*. The entire Q_{soma}, however, did not depolarize the soma because much of it flowed into the basal dendrites. Note that the active dendrites did not make Q_{dend}^* perfectly uniform. This was especially apparent for very distal synapses, which showed a slight increase in Q_{dend}^* as a function of distance from the soma.

One question remaining involves the spatial distribution of charge injection for active dendrites. For a particular synapse, is dendritic charge injected only at the location of the

synapse or does the entire dendritic tree contribute charge? As Q_g^* is the sum of charge injected across the entire dendritic tree, Fig. 4*D* does not indicate the location of charge injection. Figure 4*F* shows the percent of Q_g^* that comes from the proximal, middle, and distal third of the dendrites for three different synapse locations (superposition still is being used here). The amount of charge injected by the dendrites in the same region as the active synapse was approximately one-half the total charge. The remainder came from other dendritic regions. In this model, the active dendrites functioned as a single unit with all regions contributing to a synaptic input regardless of location.

Model 1 has demonstrated that location-dependent variability can be reduced with a dendritic membrane that exhibits increased charge injection with depolarization (Fig. 4*D*). Theoretically, any voltage-dependent channel with a negative slope conductance could serve this function. This would include depolarization-activated inward currents or depolarization-inactivating outward currents. Depolarization-activated outward currents with positive slope conductances (as found in many K^+ channels) would increase the location-dependent variability. We next explored how realistic inward currents might reduce location-dependent variability by first using a simplified channel model, called I_{boost}.

Dendritic fidelity in the boosting model (model 2)

The second model was made more realistic than the previous model in three ways (see Table 2). First, the dendrites had a passive membrane ($G_{D_m} = 0.04$) on which a voltage-dependent ''artificial'' current was added. In reference to the ''boosting hypothesis'' of active dendrites, this current was named I_{boost}, and its *I-V* relationship is shown in the inset of Fig. 5*A*. On activation at -50 mV, I_{boost} was linear with the slope of the *I-V* relationship equal to the conductance, G_{boost}. I_{boost} was an instantaneous function of voltage with no time dependence. The difference between adding I_{boost} and varying G_{D_m} as in the previous simulations, was that I_{boost} more closely mimics the nonlinear activation of realistic voltage-gated inward currents. This was important for developing the final and most realistic model.

The second difference between these and the previous simulations was that instead of synapses being modeled as constant conductance changes, they were modeled realistically as synaptic trains and asynchronously activated at 50 Hz for 100 ms. To simulate an AMPA-like synaptic input, single synaptic conductance changes were modeled as alpha functions with a 2-ms time to peak and a maximum conductance of 100 pS. As in the previous model, each input pattern was chosen randomly from 1,000 synaptic locations uniformly distributed over the entire apical dendritic surface area. A third difference was the addition of Na^+ and K^+_{DR} conductances to the soma that allowed the model to produce action potentials. An example of the model's response to a synaptic input is shown in Fig. 5*A* for passive and active dendrites.

P_f curves again were used to estimate the location-dependent variability (Δ). For a range of G_{boost} values, Δ is plotted in Fig. 5*B*. As G_{boost} was made more negative, Δ decreased until a minimum was reached at -0.12 mS/cm^2. G_{boost} values more negative than -0.12 mS/cm^2 caused the dendrites to become excessively excitable and Δ increased. These results are very similar to that of the linear model. The nonlinearities of I_{boost}, however, prevented us from using superposition to compute the CV of individual synaptic inputs.

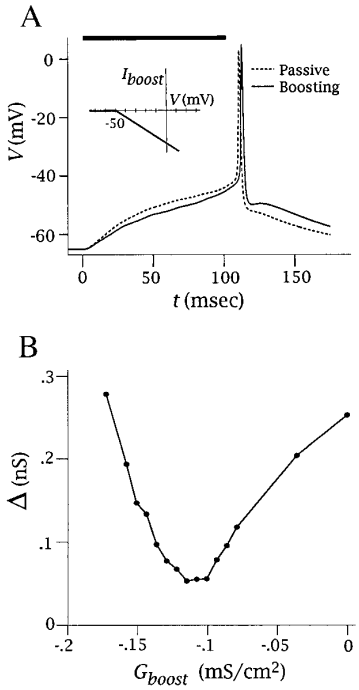

FIG. 5. Voltage-dependent current (I_{boost}) was used to minimize location-dependent variability. *A*: membrane potential (V_m) at the soma in response to a 50-Hz randomly selected synaptic input pattern for passive and boosting dendrites. For the boosting dendrites, $G_{boost} = -0.12$ mS/cm^2. Heavy bar indicates the time of synaptic input (100 ms). Number of active synapses per pattern was set to produce responses just above threshold. *Inset*: *I-V* relationship of I_{boost}, which activates at -50 mV. *B*: Δ is plotted against G_{boost}. A G_{boost} of -0.12 mS/cm^2 corresponds to the minimum Δ.

Effects of individual synaptic strength and integration time on the amount of boosting

We wanted to understand how the strength of individual synapses and duration of the synaptic input would affect the optimal value for G_{boost}. The strength of individual synapses was increased (by increasing synaptic frequency to 75 Hz) or decreased (30 Hz) while the duration was kept at 100 ms, and two new sets of P_f-curves were computed. In Fig. 6*A*, Δ is compared with the original set of curves for 50 Hz (replotted from Fig. 5). It was striking to see that the optimal value of G_{boost} did not change for the three different input conditions. The minimum Δ for each input condition corresponds to the same value of G_{boost}. Next, the effect of increasing or decreasing duration of the synaptic input was investigated. The strength of each synaptic input was maintained at 50 Hz with the duration set to 60 or 140 ms. Figure 6*B* illustrates that unlike synaptic strength, integration time affects the optimal value of G_{boost}. For a 60-ms duration, the optimal value of G_{boost} more negative than for the 100-ms integration time. The opposite effect was observed for a synaptic duration of 140 ms. These results are consistent with the idea that active dendrites provide charge compensa-

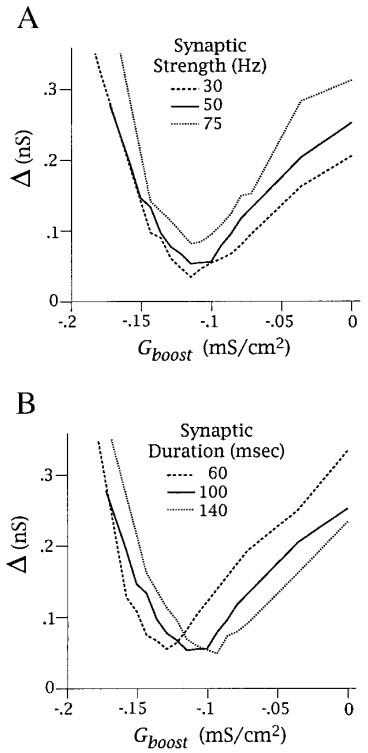

FIG. 6. Effects of individual synaptic strength and duration on the optimal value of G_{boost}. *A*: effect of varying synaptic strength on Δ. Synaptic strength was varied by increasing or decreasing the frequency of synaptic input. Optimal value of G_{boost} (that produced the minimum Δ) did not change with synaptic strength. Number of active synapses per pattern corresponding to the minimum Δ were 204, 125, and 82 for 30, 50, and 75 Hz, respectively. *B*: effect of the duration of the synaptic input on Δ. Input duration and the optimal value of G_{boost} appear to be inversely related. Number of active synapses per pattern corresponding to the minimum Δ were 162, 125, and 114 for 60, 100, and 140 ms, respectively.

tion as shown in Fig. 3. The shorter the synaptic duration, the less time the dendrites have to inject the same amount of charge, thereby requiring a larger I_{boost}.

Although we were interested primarily in observing how the optimal value of G_{boost} varied under different input conditions, there are several other aspects of Fig. 6 that deserve further discussion. Notice that in Fig. 6*A*, varying individual synaptic strength produced vertical shifts in Δ for all values of G_{boost} (especially apparent for passive dendrites with a $G_{boost} = 0$). This was due to the number of active synapses per pattern. Increasing the number of active synapses per pattern would result in smaller variability between patterns, regardless of the dendritic composition. Figure 6*B* presents a more complex situation in that two parameters are varied—the number of synapses and the synaptic duration. These two parameters have opposing effects on Δ. Because our measure of Δ is based on G_{syn}, it does not account for the change in synaptic effectiveness that accompanies a change in synaptic duration. For example, in Fig. 6*B*, increasing duration to 140 ms also increased the amount of charge injected for each synapse even though the individual synaptic conductances had not changed. This resulted in a decrease in Δ that counteracted the effect of decreasing the number of active synapses (which alone would increase Δ).

Using realistic voltage-gated channels to improve dendritic fidelity (model 3)

A major limitation of the simulations described above is that the artificial current I_{boost} was modeled using a simplified negative conductance G_{boost}. In the third model, T-type Ca^{2+} (I_{CaT}) and persistent Na^+ (I_{NaP}) channels were used to test the hypothesis that voltage-gated inward currents could serve the role of the negative conductance channel I_{boost}.

Realistic currents were numerically fit to I_{boost} (see APPENDIX). Figure 7*A* illustrates the fitted channel densities for apical dendrites containing T-type Ca^{2+} channels, persistent Na^+ channels, or both T-type Ca^{2+} and persistent Na^+ channels. The channel densities are not uniform but vary as a function of distance from the soma. This was especially apparent when the two channels were fitted simultaneously. The reason for this nonuniformity is that each dendritic compartment operates under a different voltage range when receiving a synaptic input (see Fig. 3). The *insets* in Fig. 7*A* show sample somatic responses for each model. For dendrites containing T-type Ca^{2+} channels, the model also exhibited bursting behavior.

Just as G_{boost} had an optimal value that minimized Δ, so did the realistic conductances. The density in each dendritic compartment was scaled up or down with a constant multiplier, which we called a ''density scale factor.'' Δ is plotted in Fig. 7*B* for both increases and decreases in the channel densities. A density scale factor of 1 corresponds to the

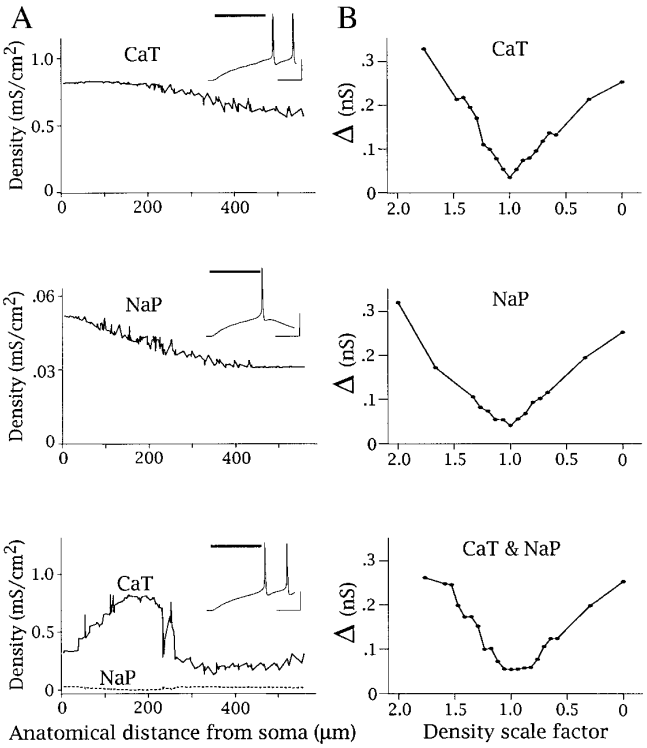

FIG. 7. I_{CaT} and I_{NaP} decrease location-dependent variability. *A*: density of realistic conductances as a function of distance from the soma. Densities reported correspond to the minimum Δ. *Inset*: somatic voltage response to synaptic input (heavy bar) adjusted for each model to be just above threshold. Scale bar is 20 mV and 50 ms. *B*: Δ plotted against the scaled channel densities of the realistic models. A density scale factor of 1 corresponds to the densities shown in *A*.

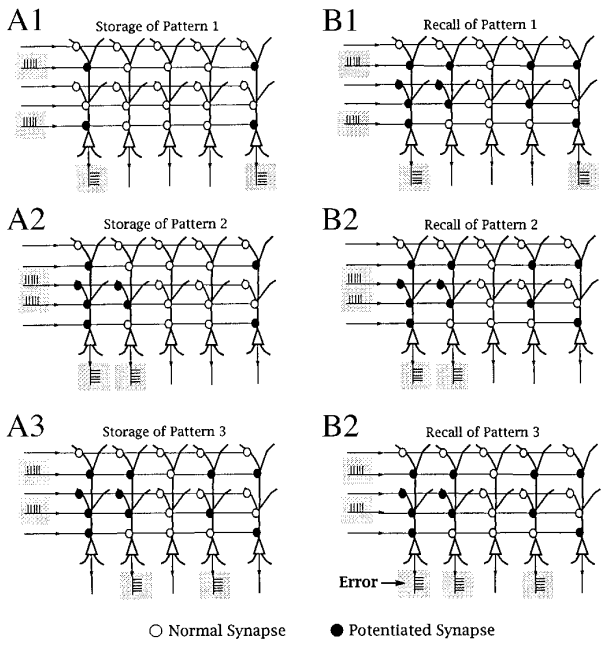

FIG. 8. Demonstrating the heteroassociative memory network. A simple network consisting of 5 cells with 5 synaptic inputs per cell. Unpotentiated synapses are represented as ○ and potentiated synapses as ●. Activity is represented by one or more action potentials (| | |). Sequence of storing and recalling 3 associative patterns of activity is illustrated. *A, 1–3*: storage of 3 associations. *A1*: first association is stored by potentiating the 4 synapses that have a coincident pre- and postsynaptic activity. *A2*: storage of the second association. Notice that with the storage of each additional association, more synapses are potentiated. *A3*: storage of the third association. *B, 1–3*: after the associations have been stored, network recall is tested. *B1*: presenting the first input pattern correctly recalls the first pattern stored. *B2*: applying the second input results in correct recall of the second pattern stored. *B3*: an error, in the form of an extra cell firing, occurs when the third input pattern is applied.

densities in Fig. 7*A* that minimized Δ. A density scale factor of 0 corresponds to passive dendrites. Scaling the fitted densities up or down had the same effect on Δ as varying G_{boost}.

Heteroassociative memory network

A heteroassociative memory network was used to test the prediction that active dendrites could improve recall performance. The heteroassociative network (also known as the matrix memory network) has the synaptic connectivity shown in Fig. 8 and has been used as a model for the CA1 region of the hippocampus (McNaughton 1989; Rolls 1989). The network associates a specific pattern of input activity with a specific output pattern. Many associations can be stored simultaneously, giving the network the property of distributed memory. Potentiation of synaptic connections was the mechanism for storing associations. A simplifying assumption in our network simulations was that the input and output patterns were binary. Cells were considered either to be firing or silent. This imposed binary coding scheme allowed the performance of the network to be quantified easily.

A simple example of how the heteroassociative memory network stores associations is shown in Fig. 8. In this example, five cells each receive a single synapse from five afferent fibers. A synapse is represented as a small circle. Open circles indicate an unpotentiated synapse and filled circles a potentiated synapse. Synapses are potentiated based on coincident pre- and postsynaptic activity. Once a synapse is potentiated, it does not become unpotentiated. Initially, the network contains no potentiated synapses. In Fig. 8*A, 1–3,* three associations are stored. After all the associations are stored, the network is tested (Fig. 8*B, 1–3*). Each input pattern results in accurate recall of its corresponding output pattern except for *pattern 3,* which produces an error in the form of an additional cell firing. This example illustrates an important network feature. As more patterns are stored, the probability of producing errors is increased. Thus network capacity can be defined in terms of the probability of producing an error (Palm 1980).

For our network simulations, we used the proportion of cells that fired correctly (P_S) in response to each stored pattern as our measure of network performance. Testing our example network resulted in 14 out of 15 cells responding correctly (Fig. 8*B, 1–3*). This produced a $P_S = 0.93$.

Active dendrites improve heteroassociative memory recall

Heteroassociative networks were constructed with the boosting model (*model 2*) and the realistic model (*model 3*) to examine how minimizing location-dependent variability affects recall performance. For comparison, a model containing a spiking soma and passive dendrites (with various dendritic R_m) also was used. The prediction was that networks constructed with models containing active dendrites would outperform the passive dendrite models.

A heteroassociative network similar to the one in Fig. 8 was simulated using 10 realistic cells and 1,000 afferent input lines. The number of active inputs per pattern was determined by the threshold of the particular model used, which was set to fire the particular model 98% of the time in response to a fully potentiated synaptic input. There were always five output cells active per pattern. The activity of the input was modeled as a 50-Hz synaptic train for 100 ms. Input and output patterns were selected randomly. Synapses were modeled with alpha functions with a peak conductance of 50 pS for an unpotentiated synapse and 100 pS for a potentiated synapse. To compare the different models, the effect of the different thresholds had to be taken into account. The number of patterns stored was a function of the number of active input lines per pattern. For each network, the number of patterns stored always was set to produce $P_S = 0.95$ in an equivalent network constructed of ideal threshold units (see APPENDIX). This equivalent network had the same number of cells, active synapses per pattern, and number of patterns stored as the realistic network. Ideal threshold units have a $\Delta = 0$ and therefore provide the basis with which to evaluate the realistic network's performance. Associations between the input and output patterns were stored by potentiating the appropriate synapses. The network then was tested by replaying the complete set of input patterns and observing the output to calculate P_S.

It was demonstrated previously that increasing R_m in passive dendrites only slightly decreased the location-dependent variability of the synaptic input (see Fig. 1). Figure 9*A* shows the results from a heteroassociative network with neurons that have passive dendrites. The dendritic R_m was varied

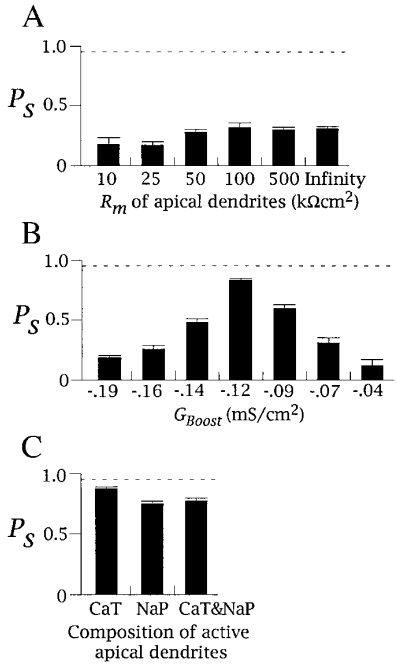

FIG. 9. Heteroassociative network performance with passive (*A*) and active dendrites (*B* and *C*). Each bar represents the proportion of cells that fired correctly (P_S) during recall of a 10-cell associative matrix memory network (average of 3 network simulations). Number of patterns stored for each network was set to produce $P_S = 0.95$ in an ideal threshold model, which had no location-dependent variability (– – –). *A*: networks were simulated with passive dendrites with different dendritic R_m. Increasing R_m only marginally enhances performance with passive dendrites. Dendritic R_m was varied from 10 kΩ cm^2 to ∞. *B*: networks simulated with the boosting model (*model 2*). Performance as a function of G_{boost}. With $G_{boost} = -0.12$ mS/cm^2, the model's performance is near maximal. G_{boost} was scaled from −0.19 to −0.04 mS/cm^2. Dendritic R_m for the boosting model was 25 kΩ cm^2. *C*: network performance for the 3 realistic models (*model 3*). Densities used are those shown in Fig. 7*A*. Moving *left* to *right*, the number of active synapses per pattern and the number of patterns stored (in parenthesis), for each bar is: *A*, 266 (27), 161 (43), 128 (53), 112 (58), 100 (65), and 97 (67); *B*, 110 (59), 116 (58), 120 (56), 125 (53), 130 (52), 137 (50), and 149 (46); *C*, 117 (57), 124 (55), and 119 (56). Error bars are SE.

from 10 kΩ cm^2 to infinity. Compared with the 95% performance level of the perfect threshold model, no passive model performed well. These simulations indicate that simply eliminating the leak conductance (i.e., increasing R_m) results in only marginal improvement in performance.

The effect of active dendrites on network performance was examined using *model 2* by varying the value of G_{boost} (Fig. 9*B*). As previously demonstrated in Fig. 5, dendrites containing I_{boost} showed an improved ability to eliminate synaptic location as a component of the input. A G_{boost} of −0.12 mS/cm^2 gave the best network performance. ($G_{boost} = -0.12$ also minimized Δ in Fig. 5.) Notice in Fig. 9*B*, that when G_{boost} was made less negative, the dendrites became more passive, and network performance degraded. As G_{boost} was made more negative than −0.12 mS/cm^2, the dendrites became hyperexcitable, which also impaired network performance.

Figure 9*C* shows the performance of the three realistic models in the heteroassociative network. The channel densities of each model are as shown in Fig. 7*A*. Realistic active dendrite models had improved recall performance as compared with the passive model.

DISCUSSION

The hypothesis that dendritic voltage-gated channels counteract cable properties and minimize the effect synaptic location has on somatic depolarization was addressed. Correctly setting a single conductance (either G_{D_m} or G_{boost}) to the appropriate value greatly reduced location-dependent variability. Dendritic T-type Ca^{2+} and persistent Na^+ currents functioned as well as I_{boost} but required nonuniform channel densities. Recent experimental evidence suggests both dendritic T-type Ca^{2+} and persistent Na^+ are capable of boosting EPSPs in hippocampal neurons (Gillessen and Alzheimer 1997; Lipowsky et al. 1996).

Our earlier simulation results reported that voltage-gated channels in dendrites increased location-dependent variability (Cook et al. 1994). These results, however, were due to channel densities that did not provide the optimal *I-V* relationship in the dendrites. As demonstrated here, dendrites that are too active can amplify the effect of location on synaptic input.

The realistic channel densities required to reproduce I_{boost} were usually less than those reported by Magee and Johnston (1995) in dendritic patches. For example, the authors reported that low-voltage–activated Ca^{2+} channels have a dendritic density of ~1 mS/cm^2. The model containing only T-type Ca^{2+} channels had an average density of ~0.75 mS/cm^2. The model that also included the persistent Na^+ channels required a slightly lower average T-type Ca^{2+} density (~0.5 mS/cm^2). The discrepancy between the model and experimental data may be attributed to the lack of depolarization-activated dendritic K^+ channels (Hoffman et al. 1997). The only positive slope conductance in the dendrites of our models was the leak conductance. Adding such K^+ channels to the dendrites would increase the required densities of the fitted inward currents.

Other voltage-gated channel models were used to mimic I_{boost} (data not shown). Both the transient Na^+ and the N-type Ca^{2+} currents reduced location-dependent variability, but had slightly lower performance than I_{boost}. The L-type Ca^{2+} current, however, was completely incapable of reducing location-dependent variability because of its high-voltage threshold for activation. It also should be emphasized that the realistic channel models are not mechanistically equivalent to the negative conductance of I_{boost}. Realistic voltage-gated channels have positive instantaneous *I-V* relationships. The ability to produce the same negative *I-V* trajectories as I_{boost} is dependent on the relative rates of channel activation and change in membrane potential.

The kinetics of the I_{CaT} model differed substantially from the kinetics of the I_{NaP} model. I_{CaT} had voltage-dependent inactivation whereas the I_{NaP} model was noninactivating. Also, the rate of activation for I_{CaT} was more than an order of magnitude slower than that of I_{NaP}. Due to these differences, the fitted density of the T-type Ca^{2+} conductance was ~10 times higher than the noninactivating persistent Na^+ conductance (Fig. 7). The simulations presented here show that as long as the channels provided a net negative slope conductance that allowed the correct amount of charge to enter the dendrites, location-dependent variability was reduced. These simulations predict that any collection of voltage-dependent channels that meet this requirement also would serve this function.

The heteroassociative memory network was used to demonstrate how active dendrites can improve network function. In these simulations, active dendrites dramatically improved memory recall. With optimal densities of voltage-gated channels in the dendrites, the soma is better able to estimate the strength of the synaptic input. This improved fidelity allows the cells to decide more accurately whether or not to fire an action potential. Accurate firing of individual cells leads to improved overall network performance. The heteroassociative network simulations provide an interesting link between dendritic physiology and memory performance. Preliminary results (not shown) have suggested other neural network architectures, such as the autoassociative network, also would benefit from dendrites that minimize location-dependent variability.

By minimizing Δ, we improved on the passive dendrite model's ability to store any general set of patterns. It is interesting to imagine a different scenario where information is not only stored in the synaptic strength but also in the composition of the active dendrites. In this way, the dendrites might be tuned to further enhance the storage of information beyond that demonstrated in our network simulations.

Assumptions of the model

In establishing that active dendrites could improve the fidelity of transmission of synaptic input to the soma, several important assumptions were made: *1*) hippocampal pyramidal neurons are temporal integrators. The most fundamental assumption underlying this study is that synaptic input is integrated in the soma where the decision to fire an action potential is made. These simulations assumed that neurons integrate the synaptic input on the order of tens of milliseconds. Therefore, the effect of active dendrites on single EPSPs was not considered. *2*) All synapses are the same. This is an oversimplification, as there are cases of specialized synaptic inputs to central neurons (e.g., the mossy fiber input to hippocampal CA3 cells). *3*) Patterns of activity were selected randomly. At present it is entirely unknown how patterns of activity impinge on hippocampal neurons. *4*) Only AMPA-like synapses were used. *N*-methyl-D-aspartate (NMDA) synaptic inputs provide a negative slope conductance and theoretically could reduce location-dependent variability. *5*) Only threshold properties were explored in the models. The continuous firing properties of the models were not addressed. In vivo single-unit recordings have shown that hippocampal pyramidal neurons have low firing rates and a tendency to fire in bursts (Ranck and Feder 1973). *6*) No synaptic background noise was included; this may affect active dendrites more than passive (De Schutter 1995). And, *7*) minimizing location-dependent variability of the synaptic input was the only dendritic function considered. Accurately transmitting synaptic input to the soma is one of several important functions dendrites perform. Dendrites also regulate plasticity through Ca^{2+} entry (Bliss and Collingridge 1993), the transmission of backpropagating action potentials (Magee and Johnston 1997; Spruston et al. 1995), and burst firing (Wong and Prince 1978). It is interesting to note, however, the model that maximized fidelity with dendritic T-type Ca^{2+} channels also produced burst firing.

Implications of negative dendritic slope conductances

Depending on the sign and slope of the dendritic *I-V* relationship, three basic ''dendritic modes of operation'' can be described. *1*) A positive slope *I-V* relationship. This is the passive case in which current escapes across the membrane conductance. This mode has high location-dependent variability. *2*) A negative slope *I-V* relationship that is stable. Here, active dendrites inject current but do not regeneratively depolarize. In this mode, location-dependent variability is reduced. *3*) A negative slope *I-V* relationship of sufficient magnitude to produce regenerative depolarizations with location-dependent variability greatly increased. The transition point at which an active dendrite becomes regenerative depends on the relative conductances of the entire neuron (Jack et al. 1975).

Using the linear model, superposition of the synaptic inputs clearly shows that passive dendrites reduce the amount of charge reaching the soma in a distance dependent fashion. The three sources for this interference are: the accumulation of charge on dendritic membrane capacitance, the escape of charge across synaptic and nonsynaptic dendritic membrane conductances, and the reduction in synaptic charge entry due to increased depolarization of dendrites located farther from the soma. Active dendrites compensate for this by making either the total charge lost or accumulated by the dendrites more uniform. The only way to ensure that active dendrites inject more charge distally is to have a negative slope *I-V* relationship. It is important to emphasize that active dendrites did not eliminate synaptic charge loss and accumulation, but rather made the amount more equivalent for all synapses, independent of their location. Superposition also demonstrated that the entire dendritic tree contributes to every synapse when increasing dendritic fidelity.

None of the models eliminated all location-dependent variability. To do this, distal portions of the dendrites may require an increased boosting current. This might be accomplished by making the dendritic *I-V* relationship nonlinear (as is the case for realistic voltage-gated currents) or regionally varying G_{D_m} and G_{boost}.

Other models of active dendrites

It has been suggested that voltage-dependent currents could alter the integrative properties of dendrites (Jack et al. 1975). The idea that active dendrites boost weaker distal inputs has been speculated, especially as a role for active spines (Miller et al. 1985; Perkel and Perkel 1985; Shepherd et al. 1985). In general, any voltage-gated current producing a negative slope conductance (either depolarization-activated inward or depolarization-inactivated outward currents), in dendrites or spines, will amplify the synaptic input. If dendrites are to act as high-fidelity transmitters of synaptic input, the amount of amplification is critical. This study attempted to regulate carefully the amount of dendritic amplification to allow all synapses to be electrically equidistant from the soma.

Most recent quantitative models propose that dendrites actively participate in neuronal computation. To the contrary, the boosting model outlined here proposes that dendrites do not contribute to the computation and instead provide the soma with an accurate estimate of the magnitude of

synaptic input. This model also suggests that active dendrites function as a single unit and not as separate regions or local subunits (Wilson 1995; Woolf et al. 1991).

Mel (1993) has proposed that active dendrites detect spatial clustering of synaptic activity. Although not tested here, it is likely that in addition to maximizing dendritic fidelity, the active dendrites constructed from realistic currents also would have some cluster sensitivity. The nonlinear *I-V* relationships of the Ca^{2+} and Na^{+} channels would allow spatially clustered inputs to inject more charge than spatially diffuse inputs.

One component of location-dependent variability is a reduced synaptic driving force as a function of distance from the soma. Bernander et al. (1994) demonstrated that dendritic K^{+} channels could linearize the effects of driving force. Their study differed significantly from ours in that they addressed the problem in terms of driving force versus synaptic strength. It would be impossible for any such dendritic voltage-gated K^{+} channels to alone reduce location-dependent variability. The authors did mention, however, that the functional properties of their K^{+} channel model might be replicated using a voltage-gated inward current.

Location-dependent variability was minimized under the assumption that the window of integration was many tens of milliseconds. This fits well under the hypothesis that short bursts of action potentials are the primary unit of communication between neurons (Lisman 1997). It also has been proposed that central neurons may act as coincidence detectors that integrate the synaptic input over extremely short durations of a few milliseconds (Softky and Koch 1993), though this is somewhat controversial (Shadlen and Newsome 1994). To be a coincidence detector, dendrites would be required to either have a relatively fast time constant (i.e., be very passive) or be extremely nonlinear (i.e., produce regenerative depolarizations). Both would allow dendrites to be sensitive to simultaneously arriving EPSPs. Such mechanisms are on the extreme ends (either highly passive or highly active) of the three possible modes for dendritic operation. The dendritic mechanisms proposed here to maximize dendritic fidelity do not shorten the membrane time constant (in fact the time constant is increased substantially) or initiate regenerative dendritic spikes. It is unlikely that our model of active dendrites (a model that reduces location-dependent variability) would act as a coincidence detector using a small window of integration as demonstrated in other models (Jaslove 1992; Softky 1994).

We have not specifically addressed the electrotonic structure (in terms of space constants or attenuation) of our active dendrites. There have been several interesting studies of the electrotonic structure of passive dendrites (O'Boyle et al. 1996; Tsai et al. 1994; Zador et al. 1995). The methods developed to study passive dendrites, however, do not directly extend to nonlinear dendrites that contain voltage-dependent currents. The modification of existing methods or the development of new methods to explore nonlinear electrotonic structure will greatly aid in the understanding of how active dendrites influence synaptic integration.

APPENDIX

Channel kinetics

The I_{Na} model was based on voltage-clamp measurements by C. M. Colbert (unpublished observations). The I_{KDR} model was based on similar models (Migliore et al. 1995) to produce good spike repolarization when used with the I_{Na} model. These models where produced by M. Migliore and follow the general Hodgkin-Huxley formalism. For a state variable x that represents a gating particle

$$x = x_\infty - (x_\infty - x_0)e^{-t/\tau_x}$$

where $x_\infty = 1/(1 + \alpha_x)$ is the steady state value; x_0 is the initial value; and τ_x is the time constant where

$$\tau_x = \begin{cases} \dfrac{\beta_x}{q_{10} c_{0_x}} & \text{if} \quad \tau_x > \bar{\tau}_x \\ \bar{\tau}_x & \text{otherwise} \end{cases}$$

and $q_{10} = 1.5^{(T_{emp}-24)/10}$. For all simulations, $T_{emp} = 30°C$, $E_{Na} = 55$ mV, and $E_K = -91$ mV.

I_{Na} model

$$I_{Na} = \bar{g}_{Na} n^3 l (V - E_{Na})$$

$$\alpha_n = e^{(0.001 z_n (V - V_{1/2_n}) F/RT)}$$

$$\beta_n = e^{(0.0005 z_n (V - V_{1/2_n}) F/RT)}$$

$$c_{0_n} = \alpha_{0_n} + \beta_{0_n} \alpha_n$$

$$\alpha_l = e^{(0.001 z_l (V - V_{1/2_l}) F/RT)}$$

$$\beta_l = e^{(0.0005 z_l (V - V_{1/2_l}) F/RT)}$$

$$c_{0_l} = \frac{\alpha_{0_l}}{l_\infty}$$

where $\alpha_{0_n} = 2$; $\beta_{0_n} = 2$; $\bar{\tau}_n = 0.04$; $z_n = -5$; $V_{1/2_n} = -35$; $\alpha_{0_l} = 0.08$; $\bar{\tau}_l = 1$; $z_l = 4$; $V_{1/2_l} = -45$; V is membrane voltage (millivolts); F is the Faraday's constant; R is the gas constant; and T is the absolute temperature ($T_{emp} + 273.16$).

I_{NaP} model

$$I_{NaP} = \bar{g}_{NaP} n^3 (V - E_{Na})$$

This model has the same n as I_{Na} except $V_{1/2_n} = -48$.

I_{KDR} model

$$I_{KDR} = \bar{g}_{K_{DR}} m h (V - E_K)$$

$$\alpha_m = e^{(0.001 z_m (V - V_{1/2_m}) F/RT)}$$

$$\beta_m = e^{(0.0004 z_m (V - V_{1/2_m}) F/RT)}$$

$$c_{0_m} = \alpha_{0_m} + \beta_{0_m} \alpha_m$$

$$\alpha_h = e^{(0.001 z_h (V - V_{1/2_h}) F/RT)}$$

$$\beta_h = e^{(0.001 z_h (V - V_{1/2_h}) F/RT)}$$

$$c_{0_h} = \alpha_{0_h} + \beta_{0_h} \alpha_h$$

where $\alpha_{0_m} = 0.03$; $\beta_{0_m} = 0.03$; $\bar{\tau}_m = 0.2$; $z_m = -5$; $V_{1/2_m} = -32$; $\alpha_{0_h} = 0.001$; $\beta_{0_h} = 0.001$; $\bar{\tau}_h = 0$; $z_h = 2$; $V_{1/2_h} = -61$.

Numerically fitting realistic currents to I_{boost}

A least-squares minimization algorithm called PRAXIS (Brent 1972) included with the NEURON simulation package was used to fit T-type Ca^{2+} and persistent Na^{+} currents to the artificial negative slope conductance current I_{boost}. The dendrites contained

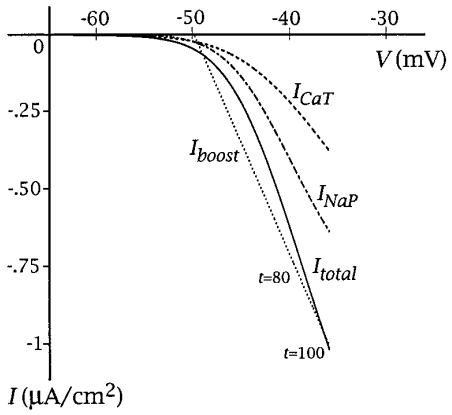

FIG. A1. Example of fitting 2 realistic currents to I_{boost} in a distal dendritic compartment. *I-V* trajectory of I_{boost}, I_{NaP}, I_{CaT}, and I_{total}, where $I_{total} = I_{CaT} + I_{NaP}$ are shown for the 100-ms synaptic input. Time is implicit with $t = 80$ and 100 ms indicated. Only the last 10 ms were used to fit the realistic currents to I_{boost}.

a passive leak ($R_m = 25\ k\Omega cm^2$) and a G_{boost} of $-0.072\ mS/cm^2$. G_{boost} was slightly less than the optimal value previously used because a uniform constant conductance synaptic input was used to provide a smooth depolarizing effect on the model. Using a synaptic train as input would have made the numerical fitting difficult because membrane potentials fluctuated with the constant change in synaptic conductance. After determining the channel densities, however, the realistic current models were tested using the standard 50-Hz synaptic trains. Replacing the artificial I_{boost} with a more realistic model proceeded one compartment at a time. Starting at the most distal dendritic compartment, I_{boost} was replaced with the type of channel (or channels) being fit. PRAXIS then was used to minimize the least-squares difference between the realistic current's *I-V* trajectory and that of I_{boost} during the last 10 ms of the synaptic input. An example of a fit using both I_{CaT} and I_{NaP} is illustrated in Fig. A1 for a distal dendritic compartment located $\sim 500\ \mu m$ from the soma. Once a best fit had been found by PRAXIS, the conductance of the realistic current (or currents) was used as the initial condition to fit the next dendritic compartment. Only the dendritic compartment being fit contained the realistic channel models, all others contained I_{boost}. Goodness of fit was monitored graphically and computed as the sum of the least-squares difference of the fit for all the compartments, with each compartment being weighted as its percentage of the apical dendrites surface area. Although this method of fitting current versus voltage produced realistic active dendrites that minimized the location-dependent variability as well as I_{boost}, we speculate that other methods of fitting (e.g., current vs. time or even total injected charge vs. time) would have produced similar results.

Binary heteroassociative network

To allow comparison between the biophysical models, we had to compensate for the effect of different dendritic excitability. Depending on the dendritic composition, some models required a smaller G_{syn} to produce an action potential. Therefore the number of patterns stored was a function of the number of active input lines per pattern. This was accomplished with the aid of a heteroassociative network constructed of simple binary threshold neurons. This network was used to determine how many patterns should be stored for a given number of active inputs. For each realistic network, the number of patterns stored was always set to produce a $P_S = 0.95$ in the corresponding network constructed from the ideal binary units.

The output of the jth (where $j = 1 \ldots 10$) ideal binary unit (y_j) was

$$y_j = \begin{cases} 1 & \text{if } \dfrac{\sum_{i=1}^{1,000} w_{ij}x_i}{T} = 1 \quad \text{where} \quad T = \sum_{i=1}^{1,000} x_i \\ 0 & \text{otherwise.} \end{cases} \tag{3}$$

where T is the threshold of the unit and is equal to the number of active inputs per pattern. The ith input is represented by x_i, which was equal to 0 for no activity or 1 for activity. The synaptic weight from the ith input to unit j is w_{ij}. Synaptic weights were either 0.5 for a nonpotentiated synapse or 1 for a potentiated synapse. Potentiation used a simple Hebbian rule and is illustrated in Fig. 8.

For a given number of active inputs and stored associations, the ideal binary network was simulated 10 times, each with a different set of randomly chosen patterns. After presenting an input pattern, the output was examined to determine the proportion of cells that fired correctly (P_S).

We thank M. Vollrath and N. Poolos for helpful comments on this manuscript. We also are grateful to M. Haque and R. Gray for computer and network support.

This work was supported by The Keck Center for Computational Biology and National Institutes of Health Grants MH-10475 to E. P. Cook and NS-11535, MH-44754, and MH-48432 to D. Johnston.

Address for reprint requests: E. P. Cook, Division of Neuroscience, Baylor College of Medicine, 1 Baylor Plaza, Houston, TX 77030.

Received 24 February 1997; accepted in final form 26 June 1997.

REFERENCES

ANDERSEN, P., SILFVENIUS, H., SUNDBERG, S. H., AND SVEEN, O. A comparison of distal and proximal dendrite synapses on CA1 pyramids in guinea pig hippocampal slices in vitro. *J. Physiol. (Lond.)* 307: 273–299, 1980.

BERNANDER, O., DOUGLAS, R. J., MARTIN, K.A.C., AND KOCH, C. Synaptic background activity influences spatiotemporal integration in single pyramidal cells. *Proc. Natl. Acad. Sci. USA* 88: 11569–11573, 1991.

BERNANDER, O., KOCH, C. AND DOUGLAS, R. J. Amplification and linearization of distal synaptic input to cortical pyramidal cells. *J. Neurophysiol.* 72: 2743–2753, 1994.

BLISS, T.V.P. AND COLLINGRIDGE, G. L. A synaptic model of memory: long-term potentiation in the hippocampus. *Nature* 361: 31–39, 1993.

BRENT, R. P. *Algorithms for Minimization Without Derivatives.* Englewood Cliffs, NJ: Prentice-Hall, 1972.

COOK, E. P., MIGLIORE, M., AND JOHNSTON, D. Neuron excitability and associative memory function. *Soc. Neurosci. Abstr.* 20: 1209, 1994.

CRILL, W. E. Persistent sodium current in mammalian central neurons. *Annu. Rev. Physiol.* 58: 349–362,1996.

DE SCHUTTER, E. Dendritic calcium channels amplify the variability of postsynaptic responses. *Soc. Neurosci. Abstr.* 20: 586, 1995.

DE SCHUTTER, E. AND BOWER, J. M. Simulated responses of cerebellar Purkinje cells are independent of the dendritic location of granule cell synaptic inputs. *Proc. Natl. Acad. Sci. USA* 91: 4736–4740, 1994.

DIRECTOR, S. W. *Circuit Theory: A Computational Approach.* New York: John Wiley, 1975.

GILLESSEN, T. AND ALZHEIMER, C. Amplification of EPSPs by low Ni^{2+}- and amiloride-sensitive Ca^{2+} channels in apical dendrites of rat CA1 pyramidal neurons. *J. Neurophysiol.* 77: 1639–1643, 1997.

HINES, M. NEURON—a program for simulation of nerve equations. In: *Neural Systems: Analysis and Modeling,* edited by F. Eeckman. Norwell, MA: Kluwer Academic Publishers, 1993, p. 127–136.

HOFFMAN, D. A., MAGEE, J. C., COLBERT, C. M., AND JOHNSTON, D. K^+ channel regulation of signal propagation in dendrites of hippocampal pyramidal neurons. *Nature* 387: 869–875, 1997.

JACK, J.J.B., NOBLE, D., AND TSIEN, R. W. *Electric Current Flow in Excitable Cells*. London: Oxford, 1975.

JAFFE, D. B., ROSS, W. N., LISMAN, J. E., LASSER-ROSS, N., MIYAKAWA, H., AND JOHNSTON, D. A model for dendritic Ca^{2+} accumulation in hippocampal pyramidal neurons based on fluorescence imaging measurements. *J. Neurophysiol.* 71: 1065–1077, 1994.

JASLOVE, S. W. The integrative properties of spiny distal dendrites. *Neuroscience* 47: 495–519, 1992.

JOHNSTON, D., MAGEE, J. C., COLBERT, C. M. AND CHRISTIE, B. R. Active properties of neuronal dendrites. *Annu. Rev. Neurosci.* 19: 165–186, 1996.

KOCH, C., POGGIO, T., AND TORRE, V. Nonlinear interactions in a dendritic tree: localization, timing, and role in information processing. *Proc. Natl. Acad. Sci. USA* 80: 2799–2802, 1983.

LIPOWSKY, R., GILLESSEN, T., AND ALZHEIMER, C. Dendritic Na^+ channels amplify EPSPs in hippocampal Ca1 pyramidal cells. *J. Neurophysiol.* 76: 2181–2191, 1996.

LISMAN, J. E. Bursts as a unit of neural information: making unreliable synapses reliable. *Trends Neurosci.* 20: 38–43, 1997.

LORENTE DE NÓ, R. AND CONDOURIS, G. A. Decremental conduction in peripheral nerve. Integration ofstimuli in the neuron. *Proc. Natl. Acad. Sci. USA* 45: 592–617, 1959.

MAGEE, J. C. AND JOHNSTON, D. Characterization of single voltage-gated Na^+ and Ca^{2+} channels in apical dendrites of rat CA1 pyramidal neurons. *J. Physiol. (Lond.)* 487: 67–90, 1995.

MAGEE, J. C. AND JOHNSTON, D. A synaptically controlled, associative signal for hebbian plasticity in hippocampal neurons. *Science* 275: 209–213, 1997.

MCNAUGHTON, B. L. Neuronal mechanisms for spatial computation and information storage. In: *Neural Connections, Mental Computations,* edited by L. Nadel, L. A. Cooper, P. Culicover, and R. M. Harnish. Cambridge, MA: MIT Press, 1989, p. 285–350.

MEL, B. W. Synaptic integration in an excitable dendritic tree. *J. Neurophysiol.* 70: 1086–1101, 1993.

MIGLIORE, M., COOK, E. P., JAFFE, D. B., TURNER, D. A., AND JOHNSTON, D. Computer simulations of morphologically reconstructed CA3 hippocampal neurons. *J. Neurophysiol.* 73: 1157–1168, 1995.

MILLER, J. P., RALL, W., AND RINZEL, J. Synaptic amplification by active membrane in dendritic spines. *Brain Res.* 325: 325–330, 1985.

O'BOYLE, M. P., CARNEVALE, N. T., CLAIBORNE, B. J., AND BROWN, T. J. A new graphical approach for visualizing the relationship between anatomical and electrotonic structure. In: *Computational Neuroscience. Trends in Research 1995,* edited by J. M. Bower. San Diego, CA: Academic Press, 1996, p. 423–428.

PALM, G. On associative memory. *Biol. Cybern.* 36: 19–31, 1980.

PERKEL, D. H. AND PERKEL, D. J. Dendritic spines: role of active membrane in modulating synaptic efficacy. *Brain Res.* 325: 331–335, 1985.

RALL, W. Branching dendritic trees and motoneuron membrane resistivity. *Exp. Neurol.* 1: 491–527, 1959.

RALL, W. Cable properties of dendrites and effects of synaptic location. In: *Excitatory Synaptic Mechanisms,* edited by P. Andersen and J.K.S. Jansen. Oslo: Universitetsforlaget, 1970, p. 175–187.

RANCK, J.B.J. AND FEDER, R. Studies on single neurons in dorsal hippocampal formation and septum in unrestrained rats. *Exp. Neurol.* 41: 461–555, 1973.

REDMAN, S. J. A quantitative approach to integrative function of dendrites. In: *International Review of Physiology: Neurophysiology II,* edited by R. Porter. Baltimore: University Park Press, 1976, vol. 10, p. 1–35.

ROLLS, E. The representation and storage of information in neuronal networks in the primate cerebral cortex and hippocampus. In: *The Computing Neuron,* edited by R. Durbin, C. Miall, and G. Mitchison. Wokingham, UK: Addison-Wesley Publishing, 1989, p. 125–159.

SCHWINDT, P. C. AND CRILL, W. E. Amplification of synaptic current by persistent sodium conductancein apical dendrite of neocortical neurons. *J. Neurophysiol.* 74: 2220–2224, 1995.

SEGEV, I. Single neurone models: oversimple, complex and reduced. *Trends Neurosci.* 15: 414–421, 1992.

SHADLEN, M. N. AND NEWSOME, W. T. Noise, neural codes and cortical organization. *Curr. Opin. Neurobiol.* 4: 569–579, 1994.

SHEPHERD, G. M. AND BRAYTON, R. K. Logic operations are properties of computer-simulated interactions between excitable dendritic spines. *Neuroscience* 21: 151–165, 1987.

SHEPHERD, G. M., BRAYTON, R. K., MILLER, J. P., SEGEV, I., RINZEL, J., AND RALL, W. Signal enhancement in distal cortical dendrites by means of interactions between active dendritic spines. *Proc. Natl. Acad. Sci. USA* 82: 2192–2195, 1985.

SOFTKY, W. Sub-millisecond coincidence detection in active dendritic trees. *Neuroscience* 58: 13–41, 1994.

SOFTKY, W. R. AND KOCH, C. The highly irregular firing of cortical cells is inconsistent with temporal integration of random EPSPs. *J. Neurosci.* 13: 334–350, 1993.

SPRUSTON, N., JAFFE, D. B., AND JOHNSTON, D. Dendritic attenuation of synaptic potentials and currents: the role of passive membrane properties. *Trends Neurosci.* 17: 161–166, 1994.

SPRUSTON, N., JAFFE, D. B., WILLIAMS, S. H., AND JOHNSTON, D. Voltage- and space-clamp errors associated with the measurement of electronically remote synaptic events. *J. Neurophysiol.* 70: 781–802, 1993.

SPRUSTON, N., SCHILLER, Y., STUART, G., AND SAKMANN, B. Activity-dependent action potential invasionand calcium influx into hippocampal CA1 dendrites. *Science* 268: 297–300, 1995.

TSAI, K. Y., CARNEVALE, N. T., CLAIBORNE, B. J., AND BROWN, T. H. Efficient mapping from neuranatomical to electrotonic space. *Network* 5: 21–46, 1994.

WILSON, C. J. Dynamic modification of dendritic cable properties and synaptic transmission by voltage-gated potassium channels. *J. Computat. Neurosci.* 2: 91–115, 1995.

WONG, R.K.S. AND PRINCE, D. A. Participation of calcium spikes during intrinsic burst firing in hippocampal neurons. *Brain Res.* 159: 385–390, 1978.

WOOLF, T. B., SHEPHERD, G. M., AND GREER, C. A. Local information processing in dendritic tree—subsets of spines in granule cells of the mammalian olfactory bulb. *J. Neurosci.* 11: 1837–1854, 1991.

ZADOR, A. M., AGMON-SNIR, H., AND SEGEV, I. The morphoelectrotonic transform: a graphical approach to dendritic function. *J. Neurosci.* 15: 1669–1682, 1995.